# Aquaporin5 Deficiency Aggravates ROS/NLRP3 Inflammasome-Mediated Pyroptosis in the Lacrimal Glands

Xin Cao,[1] Guohu Di,[1,2] Ying Bai,[1] Kaier Zhang,[1] Yihui Wang,[1] Hui Zhao,[3] Dianqiang Wang,[4] and Peng Chen[1,2]

[1]Department of Human Anatomy, Histology and Embryology, School of Basic Medicine, Qingdao University, Qingdao, Shandong Province, China
[2]Institute of Stem Cell Regeneration Medicine, School of Basic Medicine, Qingdao University, Qingdao, China
[3]The 971 Hospital of the Chinese People's Liberation Army Navy, Qingdao, Shandong Province, China
[4]Qingdao Aier Eye Hospital, Qingdao, China

Correspondence: Peng Chen, Department of Human Anatomy, Histology and Embryology, School of Basic Medicine, Qingdao University, 308 Ningxia Road, Qingdao 266071, China; chenpeng599205@126.com.
Dianqiang Wang, Qingdao Aier Eye Hospital, 519 Zhujiang Road, Qingdao 266400, China; dqw100@163.com.

XC and GD contributed equally to this work.

**Received:** October 3, 2022
**Accepted:** December 19, 2022
**Published:** January 10, 2023

Citation: Cao X, Di G, Bai Y, et al. Aquaporin5 deficiency aggravates ROS/NLRP3 inflammasome-mediated pyroptosis in the lacrimal glands. *Invest Ophthalmol Vis Sci.* 2023;64(1):4. https://doi.org/10.1167/iovs.64.1.4

**Purpose.** The pathogenesis of the lacrimal glands (LGs) is facilitated by inflammation mediated by the NACHT, LRR, and NLRP3 inflammasomes in dry eye disease. This research aimed to explore the protective effects of Aquaporin 5 (AQP5) on LGs by inhibiting reactive oxygen species (ROS) and the NLRP3 inflammasome.

**Methods.** AQP5 knockout ($AQP5^{-/-}$) mice were used to evaluate pathological changes in LGs. ROS generation was detected with a dichlorodihydro–fluorescein diacetate assay. Lipid metabolism was assessed by Oil Red O staining. The reversal of the mitochondrial membrane potential was detected using a JC-1 fluorescent probe kit. The effect of AQP5 on NLRP3/caspase-1/Gasdermin-D (GSDMD)-mediated pyroptosis was examined using pharmacological treatment of N-acetyl L-cysteine or MCC950.

**Results.** AQP5 loss significantly increased ROS generation, lipid metabolism disorders, TUNEL-positive cells, and reversal of the mitochondrial membrane potential in the $AQP5^{-/-}$ LGs. NLRP3 upregulation, increased caspase-1 and GSDMD activity, and enhanced IL-1$\beta$ release were detected in the $AQP5^{-/-}$ mouse LGs and primary LG epithelial cells. MCC950 significantly suppressed NLRP3 inflammasome-related pyroptosis induced by AQP5 deficiency in LGs and primary LG epithelial cells. Furthermore, we discovered that prestimulating the $AQP5^{-/-}$ primary LG epithelial cells with N-acetyl L-cysteine decreased NLRP3 expression, caspase-1 and GSDMD activity levels, and IL-1$\beta$ release.

**Conclusions.** Our results revealed that AQP5 loss promoted NLRP3 inflammasome activation through ROS generation. Inhibiting the ROS or NLRP3 inflammasome significantly alleviated the damage and pyroptosis of AQP5-deficient LG epithelial cells, which could provide new insights into dry eye disease.

Keywords: AQP5, ROS, NLRP3, pyroptosis, lacrimal glands

Dry eye disease (DED) is a common multifactorial eye illness. DED can be caused by tear film instability, increased tear film osmolarity, and meibomian gland dysfunction.[1,2] Ocular inflammation, which can occur in different parts of the eye, is an emerging issue.[3] The pathophysiology of many ocular diseases involves oxidative stress.[4] The inflammation and oxidative stress of the lacrimal functional unit are considered important pathophysiologic mechanisms of DED.[5–7] Thus far, the specific pathophysiological mechanism of DED has not been fully established.[6]

Aquaporins (AQPs) are transmembrane proteins that mainly transport water, glycerol, and small molecules (e.g., hydrogen peroxide [$H_2O_2$]).[8,9] The primary AQPs that transport water are AQP1, AQP2, AQP4, AQP5, AQP6, and AQP8.[10,11] Recently, several AQPs (AQP1, AQP3, AQP5, AQP8, AQP9, and AQP11) have been found to be peroxisomal pore proteins that promote the diffusion of $H_2O_2$ through lipid membranes.[12–14] AQP5 is abundantly expressed in the corneal epithelium and lacrimal glands (LGs), and it plays a critical role in lacrimal secretion.[15,16] Previous findings have shown that Sjögren syndrome is associated with selective LG defects. AQP5 trafficking may also contribute to decreased lacrimation and dry eye.[17] In addition, AQP5 enhances cell migration and proliferation and accelerates wound healing in the cornea.[18]

NACHT, LRR, and PYD domains-containing protein 3 (NLRP3) is an intracellular threat-sensing receptor that is activated by numerous pathogens and endogenous danger-related signals.[19] The NLRP3 inflammasome is also related to several ocular, human autoimmune, and inflammatory diseases, and is involved in DED pathogenesis.[20] Researchers

Copyright 2023 The Authors


This work is licensed under a Creative Commons Attribution-NonCommercial-NoDerivatives 4.0 International License.

have discovered that the NLRP3 inflammasome is increased in the ocular surface and tears of DED patients.[21] Thus, the NLRP3 inflammasome is a crucial factor in inflammatory illnesses.[20] However, the exact mechanism of DED pathogenesis is unknown.

Many studies have demonstrated that reactive oxygen species (ROS) are essential factors in NLRP3 inflammasome activation.[22] Zheng et al.[20] stated that ROS generation and NLRP3 inflammasome activation cause DED. Other studies have demonstrated that ROS-induced NLRP3 inflammasome activation increases IL-1$\beta$ bioactivity through caspase-1 activation during DED development.[20,23] It has also been suggested that ROS-induced LG oxidative stress may impair LG function in patients with DED.[24]

Pyroptosis is defined as necrotic and inflammatory-programed cell death induced by inflammatory caspases.[25] Caspase-1 activation facilitates IL-1$\beta$/IL-18 maturation. A key feature of pyroptosis is caspase-1–induced Gasdermin D (GSDMD), which has membrane pore-forming activity. GSDMD forms pores on the cell membrane surface, resulting in plasma membrane rupture and IL-1$\beta$ and IL-18 release, ultimately causing inflammatory responses.[26,27] GSDMD is considered a crucial mediator of pyroptosis.[28,29]

During our prior work, we found that AQP5$^{-/-}$ mice had a steady DED phenotype at birth and noticeable inflammation in their LGs. In this study, we discovered increased ROS content, NLRP3 inflammasome activation, and pyroptosis in the LGs of AQP5$^{-/-}$ mice. Inhibiting ROS and NLRP3 effectively decreased LG inflammation and pyroptosis. Moreover, AQP5 deficiency caused ROS accumulation in the LGs, which activated the NLRP3 inflammasome and subsequently induced pyroptosis.

## Methods

### Animals

The CRISPR/Cas9 technology was used to produce AQP5$^{-/-}$ C57BL/6 mice by Cyagen Biosciences (Guangzhou, China). All animal experiments were approved by The Ethics Committee Medical College of Qingdao University (No.QDU-AEC-2022297) and were conducted in accordance with the ARVO Statement on the Use of Animals in Ophthalmic and Vision Research.

Mice were intraperitoneally injected with MCC950 (100 µL, 20 mg/kg, TargetMol, Boston, MA, USA) once a week for 8 times in total. Then the samples were taken 1 week after the last injection of MCC950 for testing.

### Culture and Treatment of Primary LG Epithelial Cells

Mice were sacrificed by cervical dislocation after deep isoflurane-induced anesthesia (4% for induction). Their LGs were cut into small fragments (1 mm$^3$) and treated with MEM-$\alpha$ and 0.1% type 2 collagenase under shaking on a shaker at 50 rpm at 37°C for 30 minutes. After blowing and mixing, as well as centrifuging at 1000 rpm for 5 minutes, the precipitate was uniformly dissolved in Dulbecco's modified Eagle's medium containing 20% fetal bovine serum. The supernatant was discarded again, and the resulting precipitate was fully mixed with Dulbecco's modified Eagle's medium containing 20% fetal bovine serum.

We treated the primary LG epithelial cells with MCC950 (10 µM/mL; TargetMol) for 24 hours in order to inhibit the NLRP3 inflammasome. For antioxidation experiments, the primary LG epithelial cells were treated with an N-acetyl-L-cysteine (NAC) antioxidant (1 mM; Sigma, St. Louis, MO, USA) for 24 hours. Thereafter, the treated primary LG epithelial cells of passage 2 were collected for Oil Red O (ORO) staining, JC-1 staining, TUNEL staining, and Western blotting.

### Tear Measurements and Corneal Fluorescein Staining

Cotton phenol red threads were inserted into the lateral canthus of unanesthetized mice for 20 seconds, and the wet length of each eye was measured three times. The average of the three measurements was considered the tear secretion amount and used for statistical analysis. The ocular surface was stained with fluorescein solution (Sigma) and subsequently washed and inspected under the cobalt blue light (Vision Tech, Suzhou, China).

### Hematoxylin and Eosin (H&E) and Immunofluorescence Staining

The paraffin sections of LGs (4 µm) were stained with H&E and subsequently observed with a microscope. The LG cryosections or primary LG epithelial cells were fixed with 4% paraformaldehyde (Solarbio, Wuhan, China). The LG cryosections were incubated with NLRP3 (1:200; Affinity Biosciences, Cincinnati, OH, USA), caspase-1 (1:200; ABclonal, Wuhan, China), and GSDMD (1:200; Affinity Biosciences), and the primary LG epithelial cells were incubated with AQP5 (1:200; Abcam, Cambridge, MA, USA), epithelial cell adhesion molecule (1:200; Affinity Biosciences,), NLRP3 (1:200; Affinity Biosciences), caspase-1 (1:200; ABclonal), and GSDMD (1:200; Affinity Biosciences), followed by fluorescein-conjugated secondary antibodies (1:200; Life Technologies, Grand Island, NY). The cryosections were visualized using a fluorescence microscope (Olympus, Tokyo, Japan).

### ORO Staining

The LG cryosections or primary LG epithelial cells were fixed and then the cryosections were covered with ORO (distilled water: storage liquid ratio = 2:3; Cyagen Biosciences Inc.). Subsequently, the cryosections were incubated with Mayer's hematoxylin (Sigma). Gelatin sealing sheets were used for glycerol (Servicebio, Wuhan, China). The positive density was quantified using ImageJ software (version 1.52a, National Institutes of Health, Bethesda, MD, USA).

### ROS Activity and TUNEL Assay

The intracellular ROS levels were detected using a dichlorodihydro-fluorescein diacetate assay kit (Beyotime, Shanghai, China). DNA breakage was detected using a one-step TUNEL apoptosis detection kit (Beyotime). Cryosections or primary LG epithelial cells were fixed with 4% paraformaldehyde for 30 minutes. A TUNEL working solution was added to each sample, and TUNEL-positive cells were counted via microscopy.

Investigative Ophthalmology & Visual Science

### Mitochondrial Membrane Potential (MMP) Detection

The primary LG epithelial cells were incubated in RPMI-1640 medium containing 1 μ L of JC-1 (Beyotime) for 30 minutes at 37°C. Fluorescence of primary LG epithelial cells were measured using a fluorescence microscope. Under high MMP conditions, red fluorescence is produced. At low MMP, it emits a green fluorescence. Fluorescence emission changes from red to green, indicating MMP reversal.

### Western Blot Analysis

The LGs and primary LG epithelial cells were divided in a RIPA buffer, and the proteins were collected. The proteins were run and subsequently transferred to PVDF membranes. The membranes were incubated with antibodies of AQP5 (1:1000; Abcam), epithelial cell adhesion molecule (1:1000; Affinity Biosciences), NLRP3 (1:1000; AdipoGen Life Sciences, MA, USA), GSDMD (1:1000; Cell Signaling Technology, Danvers, MA), Cle-GSDMD (1:1000; Affinity Biosciences), caspase-1 (1:1000; ABclonal), Cle-caspase-1 (1:1000; ABclonal), IL-1$\beta$ (1:1000; ABclonal), Cle-IL-1$\beta$ (1:1000; ABclonal), and GAPDH (1:3000; Kangchen, Shanghai, China). The images were detected using a Tannon imaging system (Tanon 5200, Shanghai, China).

### Statistical Analyses

All results were expressed as mean ± standard error of the mean. The differences between the two groups were determined using an unpaired Student *t*-test (two-tailed). One- or two-way ANOVA was used for studies that included multiple tests. All statistical tests were bilateral, and a $P$ value of less than 0.05 was considered significant ($^{*}P < 0.05$; $^{**}P < 0.01$; $^{***}P < 0.001$). All the experimental data were analyzed using GraphPad Prism 7.0 (GraphPad Software Inc., La Jolla, CA).

## Results

### Cultivation and Identification of the Primary LG Epithelial Cells

The LGs were collected for primary culture, and the primary LG epithelial cells of passage 2 were used for observation in the experiment. In the culture system, the majority of the cells were spindle like (Fig. 1A). According to reports, both undifferentiated and differentiated epithelial cells in multiple glandular tissues are marked by the epithelial cell adhesion molecule, a marker of LG epithelial cells. A Western blot revealed that AQP5 was not expressed in the AQP5$^{-/-}$ primary LG epithelial cells, whereas epithelial cell adhesion molecule was expressed in both the wild-

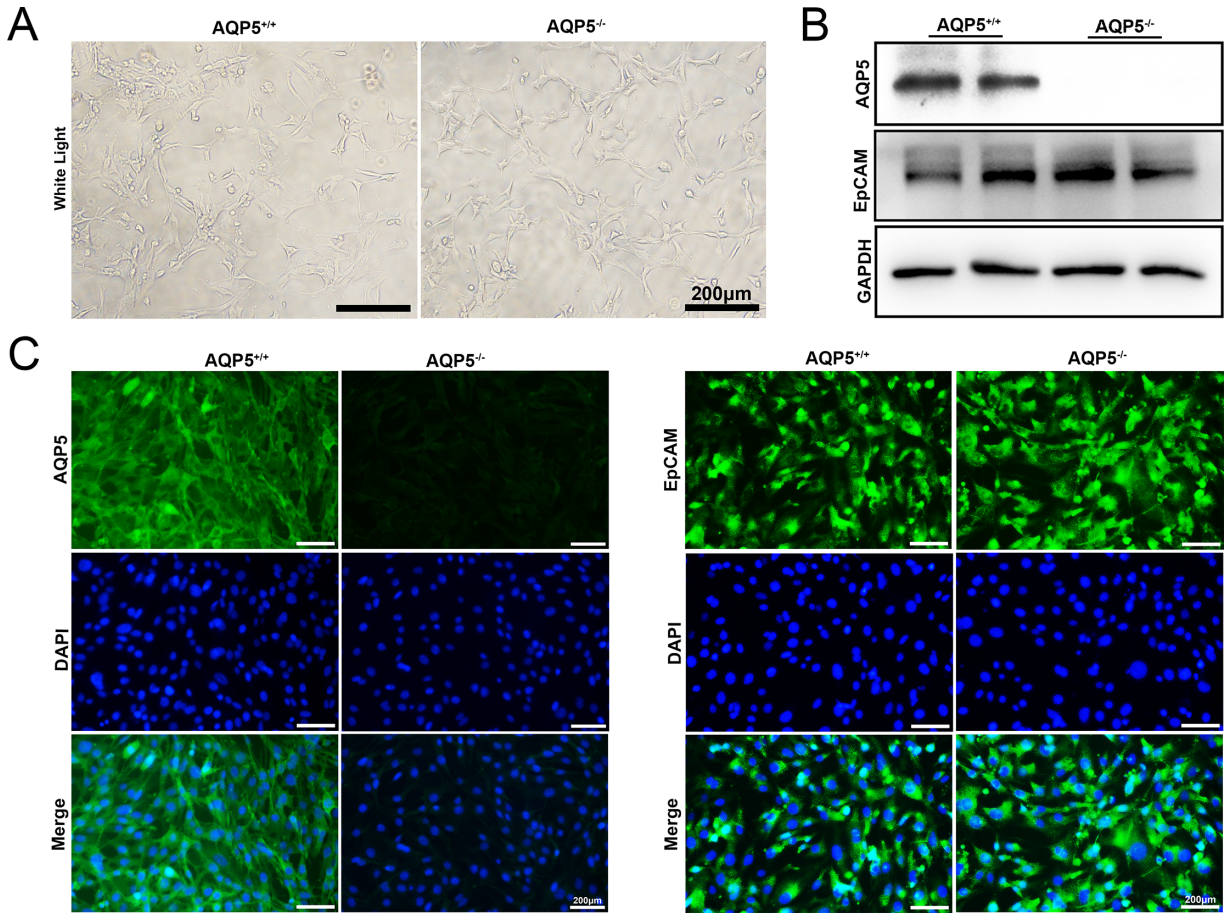


**Figure 1.** Cultivation and identification of primary LG epithelial cell. (**A**) The characteristic of primary LG epithelial cells of 1-month-old mice by culture. (**B**) Western blotting showed the expression level of AQP5, epithelial cell adhesion molecule (EpCAM) and GAPDH in primary LG epithelial cells. (**C**) Immunofluorescence staining showed the expression of AQP5 and EpCAM in primary LG epithelial cells (*green*, AQP5; EpCAM, *blue*, 4′ 6-diamidine-2-benzene index [DAPI]). (**A**, **C**) Scale bars, 200 μm.

Investigative Ophthalmology & Visual Science

type ($AQP5^{+/+}$) and $AQP5^{-/-}$ primary LG epithelial cells (Fig. 1B). Immunofluorescence staining revealed that AQP5 was detected in the primary LG epithelial cells of $AQP5^{+/+}$ mice. Epithelial cell adhesion molecule was expressed in the primary LG epithelial cells of both the $AQP5^{+/+}$ and $AQP5^{-/-}$ mice (Fig. 1C), which was consistent with the Western blotting results.

## Mitochondrial Dysfunction and Lipid Accumulation in the $AQP5^{-/-}$ Mouse LGs

H&E staining of the LGs revealed that the $AQP5^{-/-}$ mice had enlarged LG acinar cells, disordered acinar structures, and infiltrated inflammatory cells with aging (Fig. 2A). Figure 2B showed that the $AQP5^{-/-}$ mice had a significantly higher number of ROS-positive–stained primary LG epithelial cells than the $AQP5^{+/+}$ mice. The number of ROS-positive cells increased from 11 ± 0.577 in the $AQP5^{+/+}$ mice to 17.67 ± 0.882 in the 1-month-old $AQP5^{-/-}$ mice ($P < 0.01$; $n = 3$ per group), and from 40.33 ± 0.882 in the $AQP5^{+/+}$ mice to 49 ± 1.155 in the 6-month-old $AQP5^{-/-}$ mice ($P < 0.01$; $n = 3$ per group) (Fig. 2C). JC-1 staining revealed an important shift in fluorescence emission from red to green in the primary LG epithelial cells of $AQP5^{-/-}$ mice (Fig. 2D). According to the statistics, the green/red ratio of the MMP increased from 1.500% ± 0.058% in the 1-month-old $AQP5^{+/+}$ mice to 2.767% ± 0.145% in the $AQP5^{-/-}$ mice ($P < 0.05$; $n = 3$ per group) and from 13.63% ± 0.267% in the 6-month-old $AQP5^{+/+}$ mice to 15.970% ± 0.285% in the $AQP5^{-/-}$ mice ($P < 0.01$; $n = 3$ per group) (Fig. 2E).

ORO staining revealed neutral triglyceride accumulation in the acinar cells of the $AQP5^{-/-}$ mice (Fig. 2F). The neutral triglyceride intensity increased from 2574 ± 11.89 and 6681 ± 231.7 in the 1- and 6-month-old $AQP5^{+/+}$ mice, respectively, to 5348 ± 110.6 and 20,692 ± 139.9 in the 1- and 6-month-old $AQP5^{-/-}$ mice, respectively ($n = 3$ per group) (Fig. 2G). Neutral triglyceride accumulation was also detected in the primary LG epithelial cells of the $AQP5^{-/-}$ mice (Fig. 2H). The neutral triglyceride intensity increased from 2392 ± 192 and 4482 ± 204.1 in the 1- and 6-month-old$AQP5^{+/+}$ mice, respectively, to 4467 ± 217.6 and 9620 ± 283.6 in the 1- and 6-month-old $AQP5^{-/-}$ mice, respectively ($n = 3$ per group) (Fig. 2I). These results were consistent with those obtained in the LGs.

## Enhanced Pyroptosis in the LGs and Primary LG Epithelial Cells of the $AQP5^{-/-}$ Mice Owing to NLRP3 Inflammasome Activation

TUNEL staining was applied to examine DNA breakage in the LG cells (Fig. 3A). The $AQP5^{-/-}$ mouse LGs (1 month old, 0.2867 ± 0.03844%; 3 months old, 2.313% ± 0.2514%; 6 months old, 9.98% ± 1.156%; 9 months old, 35.46% ± 2.207%; 12 months old, 73.33% ± 1.202%) had a greater number of TUNEL-positive cells than the $AQP5^{+/+}$ mouse LGs (1 month old, 0 ± 0; 3 months old, 0.8733% ± 0.07688%; 6 months old, 2.6% ± 0.2594%; 9 months old, 20.67% ± 2.001%; 12 months old, 33.69% ± 2.136%; Fig. 3B). Immunofluorescence staining revealed that the $AQP5^{-/-}$ mouse LGs had higher NLRP3, caspase-1, and GSDMD expression levels than the $AQP5^{+/+}$ mouse LGs (Fig. 3C). In addition, a Western blot analysis revealed that the $AQP5^{-/-}$ mice had higher NLRP3, Cle-caspase-1, Cle-GSDMD, and Cle-IL-1$\beta$ expression levels than the $AQP5^{+/+}$ mice (Figs. 3D and 3E).

The primary cells of the mouse LGs were isolated and cultured. Primary LG epithelial cells of passage 2 were used for observation in the experiment. The TUNEL assay revealed that the $AQP5^{-/-}$ mice had more positive cells than the $AQP5^{+/+}$ mice (Fig. 4A). It also revealed that the $AQP5^{-/-}$ mice had a significantly higher number of TUNEL-positive primary LG epithelial cells than the $AQP5^{+/+}$ mice (1 month old, 1.413% ± 0.1742% vs 0 ± 0; 6 months old, 13.22% ± 0.263% vs 2.51% ± 0.1652%; $n = 3$ per group; Fig. 4B). Immunofluorescence staining revealed that the $AQP5^{-/-}$ mouse primary LG epithelial cells had higher NLRP3, caspase-1, and GSDMD expression levels than the $AQP5^{+/+}$ mouse primary LG epithelial cells (Fig. 4C). Moreover, a Western blot analysis revealed that the $AQP5^{-/-}$ mice's primary LG epithelial cells had higher NLRP3, Cle-caspase-1, Cle-GSDMD, and Cle-IL-1$\beta$ expression levels than did the $AQP5^{+/+}$ mice (Figs. 4D and 4E).

## LG Pyroptosis Reduction via NLRP3 Inflammasome Inhibition

We evaluated the effect of the NLRP3 inflammasome on the $AQP5^{-/-}$ mouse LGs by using MCC950, an NLRP3 inhibitor. Slit lamp examination revealed noticeable punctate defects in the corneas of the $AQP5^{-/-}$ mice. After injecting MCC950 intraperitoneally, the punctate defects decreased significantly (Fig. 5A), and the amount of tear secretion increased significantly (Fig. 5B). H&E staining revealed that the $AQP5^{-/-}$ mice had large LG acinar cells and disordered acinar structures, which gradually normalized in the MCC950-treated $AQP5^{-/-}$ mice (Fig. 5C). ORO staining of the LGs revealed that the acinar cells of the MCC950-treated $AQP5^{-/-}$ mice underwent a significant decrease in neutral triglyceride accumulation (Fig. 5D). The MCC950-treated $AQP5^{-/-}$ mice had a lower neutral triglyceride intensity (16,888 ± 845.7) than the $AQP5^{-/-}$ mice (38,206 ± 2454) ($P < 0.001$; $n = 3$ per group). Additionally, the MCC950-treated $AQP5^{+/+}$ mice had a lower neutral triglyceride intensity (11,327 ± 757.9) than the $AQP5^{+/+}$ mice (29,303 ± 2,000) ($P < 0.01$; $n = 3$ per group) (Fig. 5E). TUNEL staining revealed that the MCC950-treated $AQP5^{-/-}$ mice had a significantly lower number of TUNEL-positive cells (Fig. 5F). The results demonstrated that the MCC950-treated $AQP5^{-/-}$ mice (1.06700% ± 0.07219%) had a lower number of TUNEL-positive cells than the $AQP5^{-/-}$ mice (8.947% ± 0.7622%) ($P < 0.001$; $n = 3$ per group). The MCC950-treated $AQP5^{+/+}$ mice had a lower number of TUNEL-positive cells (0.6767% ± 0.1742%) than the $AQP5^{+/+}$ mice (1.79% ± 0.1015%) ($P < 0.01$; $n = 3$ per group; Fig. 5G). Furthermore, a Western blot analysis showed that MCC950 treatment significantly inhibited NLRP3 inflammation activation in the $AQP5^{-/-}$ mice and decreased their Cle-caspase-1, Cle-GSDMD, and Cle-IL-1$\beta$ levels (Figs. 5H and 5I). Overall, these results demonstrated that NLRP3 inflammasome-mediated inflammation results in LG pyroptosis in the $AQP5^{-/-}$ mice.

The primary cells of the mouse LGs were cultured and treated with MCC950. ORO staining of the primary LG epithelial cells revealed a significant reduction in neutral triglyceride accumulation in the MCC950-treated $AQP5^{-/-}$ mice (Fig. 6A). The results demonstrated that the MCC950-treated $AQP5^{-/-}$ mice had a lower neutral triglyceride intensity (3695 ± 164) than the $AQP5^{-/-}$ mice (23,150 ± 2350)

Investigative Ophthalmology & Visual Science

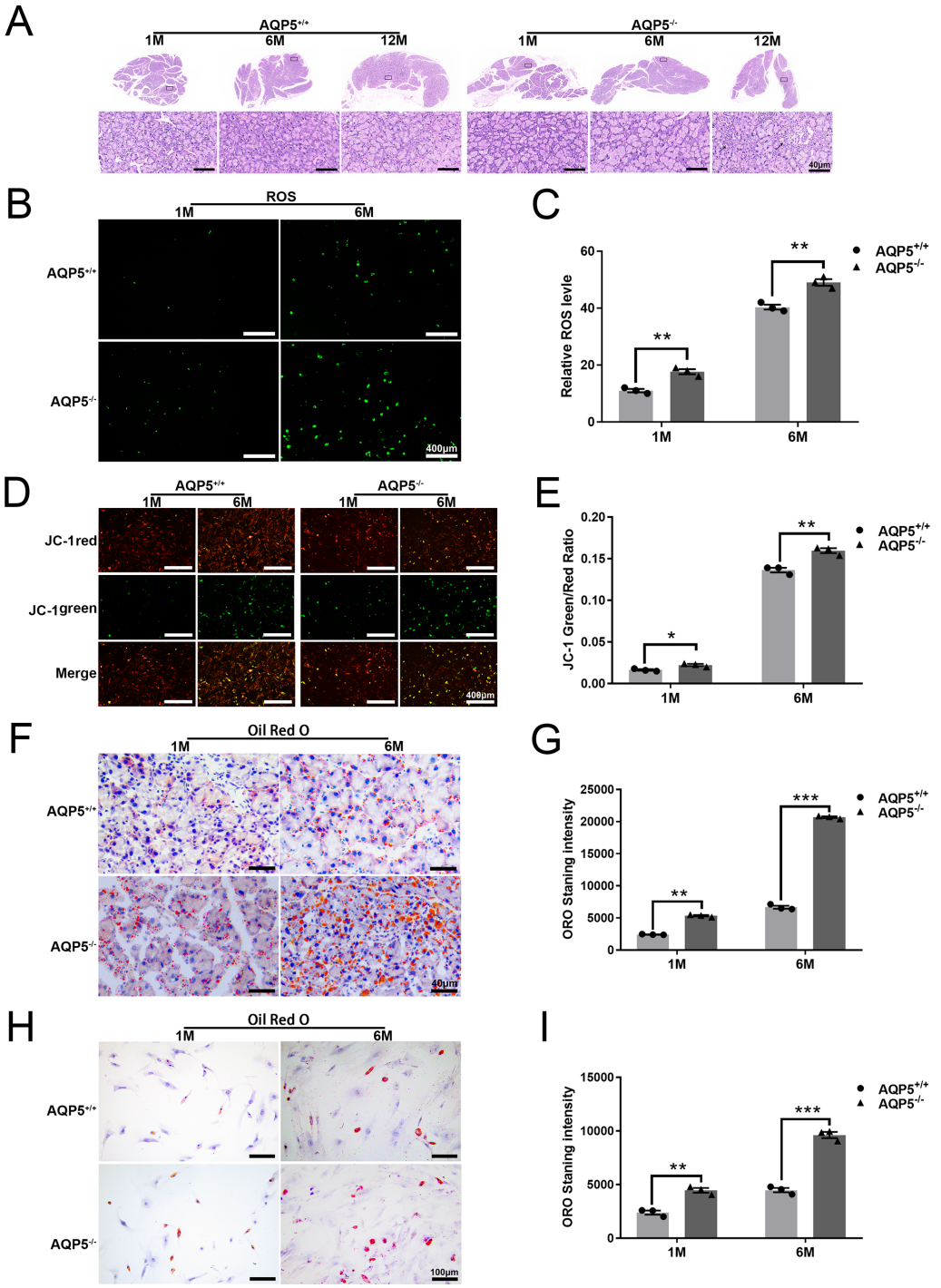


**Figure 2.** Mitochondrial dysfunction and lipid accumulation in the AQP5$^{-/-}$ mouse LGs. (**A**) H&E staining showed morphological changes and infiltration of inflammatory cells, as indicated by *black arrows*. (**B**) ROS immunofluorescence staining of primary LG epithelial cells (*green*). (**C**) ImageJ immunofluorescence spectrum analysis showed the average ROS fluorescence intensity ($n = 3$ samples). Representative complete pictures of each sample were used for quantitative analysis. The number of ROS-positive cells in the AQP5$^{+/+}$ mice (1 month old, 11 ± 0.577; 6 months old, 40.33 ± 0.882), in the AQP5$^{-/-}$ mice (1 month old, 17.67 ± 0.882; 6 months old, 49 ± 1.155). (**D**) JC-1 green/red ratio fluorescence staining of primary LG epithelial cells. (**E**) ImageJ immunofluorescence spectrum analysis showed the average fluorescence intensity of JC-1 green/red ratio ($n = 3$ samples). Representative complete pictures of each sample were used for quantitative analysis. (**F**) ORO staining of LGs ($n = 3$ samples). (**G**) ORO staining intensity analyzed by ImageJ software ($n = 3$ samples). Representative complete pictures of each sample were used for quantitative analysis. The neutral triglyceride intensity in the AQP5$^{+/+}$ mice (1 month old, 2574 ± 11.89; 6 months old, 6681 ± 231.7), in the AQP5$^{-/-}$ mice (1 month old, 5348 ± 110.6; 6 months old, 20,692 ± 139.9). (**H**) ORO staining of primary LG epithelial cells ($n = 3$ samples). (**I**) ORO staining intensity analyzed by ImageJ software ($n = 3$ samples). Representative complete pictures of each sample were used for quantitative analysis. The neutral triglyceride intensity in the AQP5$^{+/+}$ mice (1 month old, 2392 ± 192; 6 months old, 4482 ± 204.1), in the AQP5$^{-/-}$ mice (1 month old, 4467 ± 217.6; 6 months old, 9620 ± 283.6). All data are expressed as the means ± standard error of the mean. *$P < 0.05$, **$P < 0.01$, ***$P < 0.001$. Scale bars: (**A**) 40 μm, (**B, D**) 400 μm, (**F**) 40 μm, (**H**) 100 μm.

Investigative Ophthalmology & Visual Science

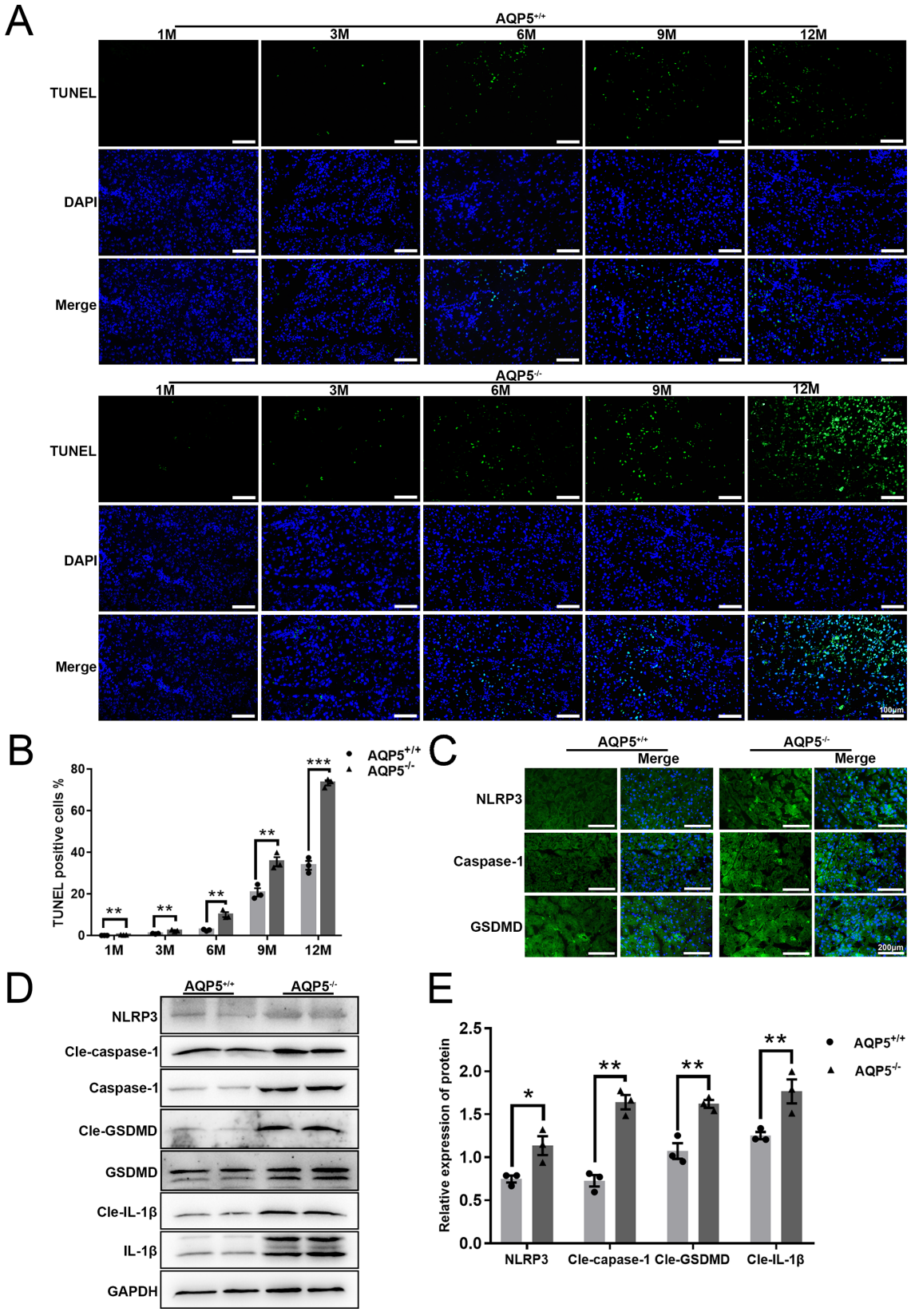


**Figure 3.** Enhanced pyroptosis in the LGs of the AQP5$^{-/-}$ mice owing to NLRP3 inflammasome activation. (**A**) TUNEL staining of LGs (*green*, TUNEL; *blue*, DAPI). (**B**) ImageJ and GraphPad were used to calculate the result of A ($n = 3$ samples). Representative complete pictures of each sample were used for quantitative analysis. (**C**) Immunofluorescence staining of NLRP3, caspase-1 and GSDMD in LGs (*green*, NLRP3, caspase-1, GSDMD; *blue*, DAPI). D: Western blotting showed the expression level of NLRP3, Cle-caspase-1, caspase-1, Cle-GSDMD, GSDMD, IL-1$\beta$, Cle-IL-1$\beta$, and GAPDH in LGs. (**E**) ImageJ and GraphPad were used to compute the result **D** ($n = 3$ samples). Data were expressed as mean ± standard error of the mean. *$P < 0.05$, **$P < 0.01$, ***$P < 0.001$. Two-way ANOVA. Scale bars: (**A**) 100 μm, (**C**) 200 μm.

Investigative Ophthalmology & Visual Science

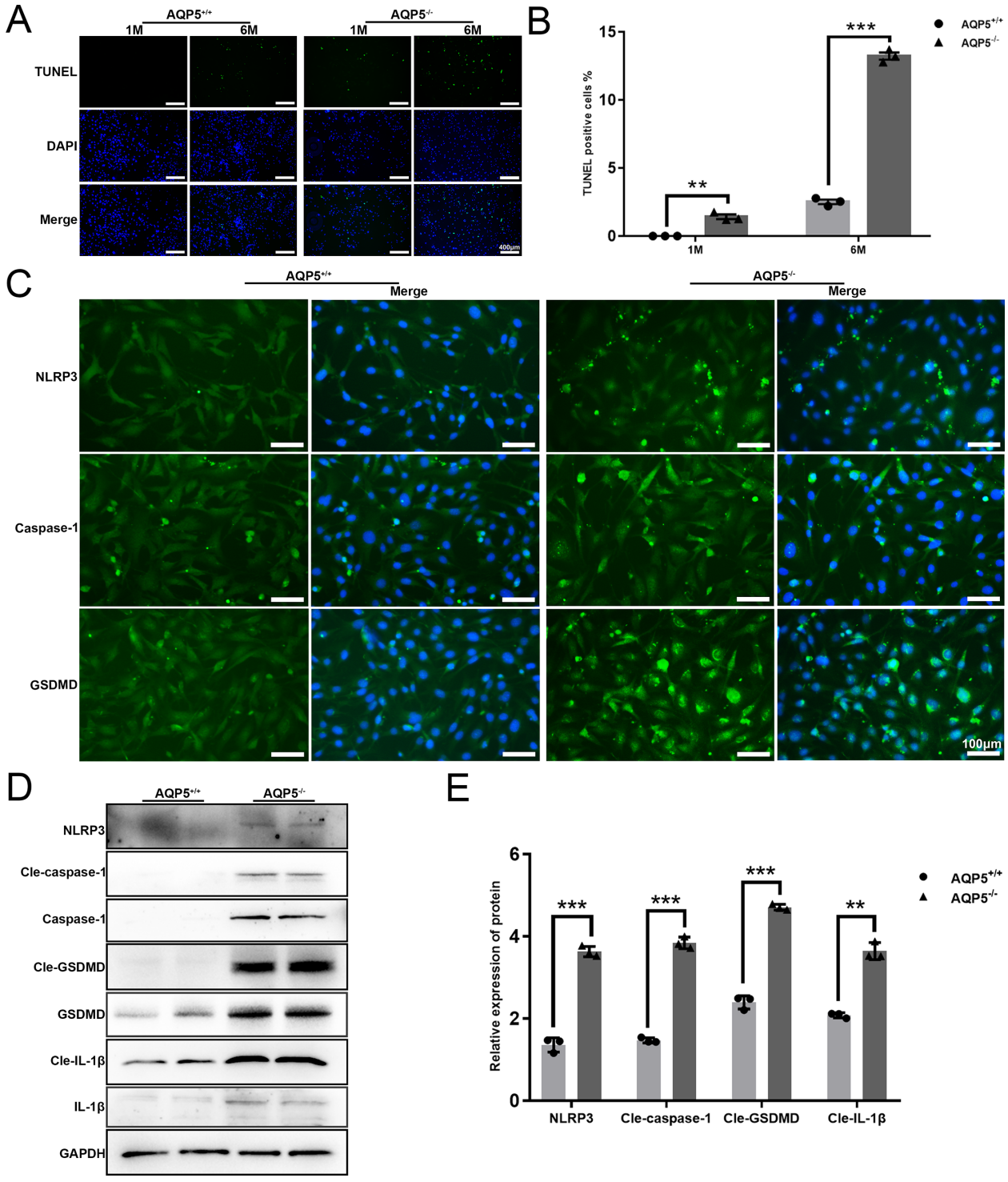


**Figure 4.** Enhanced pyroptosis in the primary LG epithelial cells of the AQP5$^{-/-}$ mice owing to NLRP3 inflammasome activation. (**A**) TUNEL staining of primary LG epithelial cells (*green*, TUNEL; *blue*, DAPI). (**B**) ImageJ and GraphPad were used to calculate the result of **A** ($n = 3$ samples). Representative complete pictures of each sample were used for quantitative analysis. (**C**) Immunofluorescence staining of NLRP3, caspase-1 and GSDMD (*green*, NLRP3, caspase-1, GSDMD; *blue*, DAPI). (**D**) Western blotting showed the expression level of NLRP3, Cle-caspase-1, caspase-1, Cle-GSDMD, GSDMD, IL-1$\beta$, Cle-IL-1$\beta$, and GAPDH in primary LG epithelial cells. (**E**) ImageJ and GraphPad were used to compute the result **D** ($n = 3$ samples). Data were expressed as mean ± standard error of the mean. *$P < 0.05$, **$P < 0.01$, ***$P < 0.001$. Two-way ANOVA. Scale bars: (**A**) 400 µm, (**C**) 100 µm.

($P < 0.001$; $n = 3$ per group) and that the MCC950-treated AQP5$^{+/+}$ mice had a lower neutral triglyceride intensity (1269 ± 101.9) than the AQP5$^{+/+}$ mice (3370 ± 248.2) ($P < 0.01$; $n = 3$ per group) (Fig. 6B). As shown in Figure 6C, the primary LG epithelial cells that alleviated the reversal of the MMP were significantly reduced

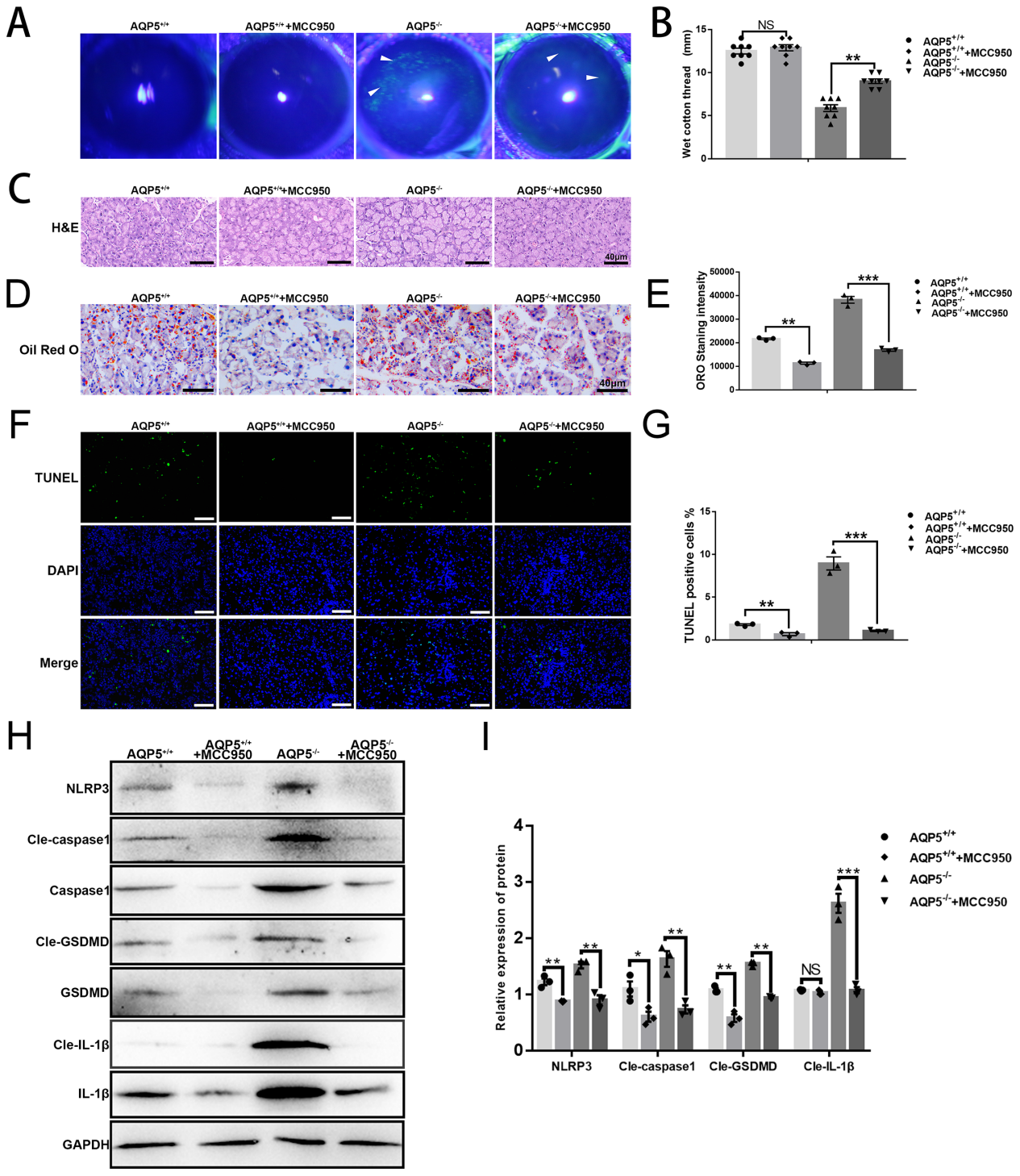


**Figure 5.** LG pyroptosis reduction via NLRP3 inflammasome inhibition. (**A**) Sodium fluorescein staining in the cornea. (**B**) The lacrimal secretion of mice was measured using the phenol red cotton thread method. (**C**) H&E staining showed morphological changes and infiltration of inflammatory cells. (**D**) ORO staining of LGs ($n = 3$ samples). (**E**) ORO staining intensity analyzed by ImageJ software ($n = 3$ samples). Representative complete pictures of each sample were used for quantitative analysis. The neutral triglyceride intensity in the $AQP5^{+/+}$ mice was 29,303 ± 2000, in the MCC950-treated $AQP5^{+/+}$ mice 11,327 ± 757.9, in the $AQP5^{-/-}$ mice 38,206 ± 2454, and in the MCC950-treated $AQP5^{-/-}$ mice 16,888 ± 845.7. (**F**) TUNEL staining of LGs (*green*, TUNEL; *blue*, DAPI). (**G**) ImageJ and GraphPad were used to calculate the result **F** ($n = 3$ samples). Representative complete pictures of each sample were used for quantitative analysis. (**H**) Western blotting showed the expression level of NLRP3, Cle-caspase-1, caspase-1, Cle-GSDMD, GSDMD, IL-1$\beta$, Cle-IL-1$\beta$, and GAPDH in LGs. (**I**) ImageJ and GraphPad were used to compute the result of H ($n = 3$ samples). Data were expressed as mean ± standard error of the mean. *$P < 0.05$, **$P < 0.01$, ***$P < 0.001$. Two-way ANOVA. Scale bars: (**C**, **D**) 40 μm, (**F**) 100 μm.

Investigative Ophthalmology & Visual Science

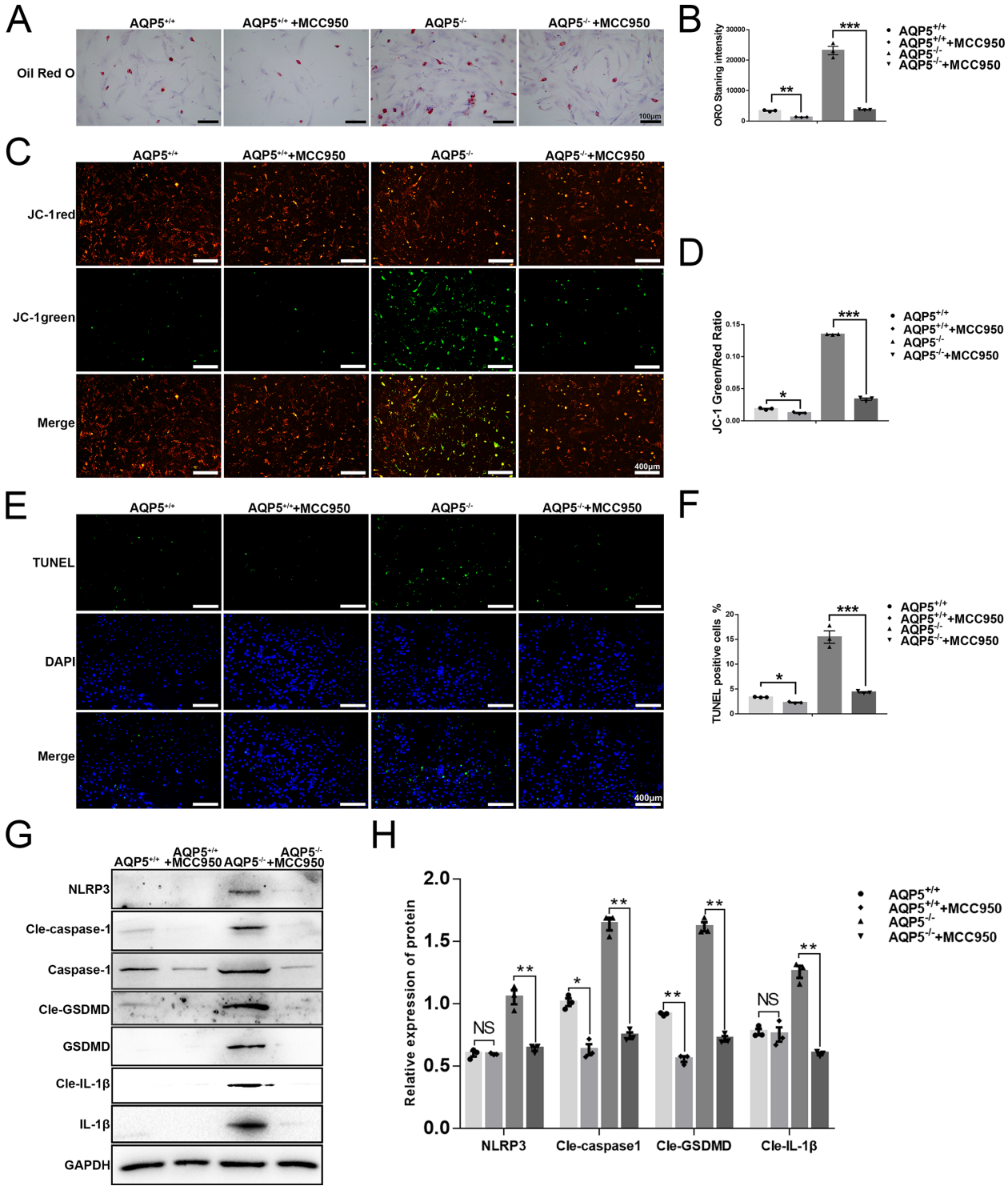


**Figure 6.** LG pyroptosis reduction via NLRP3 inflammasome inhibition. (**A**) ORO staining of primary LG epithelial cells ($n = 3$ samples). (**B**) ORO staining intensity analyzed by ImageJ software ($n = 3$ samples). Representative complete pictures of each sample were used for quantitative analysis. The neutral triglyceride intensity in the AQP5$^{+/+}$ mice was 3370.0 ± 248.2, in the MCC950-treated AQP5$^{+/+}$ mice 1269 ± 101.9, in the AQP5$^{-/-}$ mice 23,150 ± 2350, and in the MCC950-treated AQP5$^{-/-}$ mice 3695 ± 164 ($n = 3$ samples ). (**C**) JC-1 green/red ratio fluorescence staining of primary LG epithelial cells. (**D**) ImageJ immunofluorescence spectrum analysis showed the average fluorescence intensity of JC-1 green/red ratio ($n = 3$ samples). Representative complete pictures of each sample were used for quantitative analysis. (**E**) TUNEL staining of primary LG epithelial cells (*green*, TUNEL; *blue*, DAPI). (**F**) ImageJ and GraphPad were used to calculate the result **E** ($n = 3$ samples). Representative complete pictures of each sample were used for quantitative analysis. (**G**) Western blotting showed the expression level of NLRP3, Cle-caspase-1, caspase-1, Cle-GSDMD, GSDMD, IL-1$\beta$, Cle-IL-1$\beta$ and GAPDH in primary LG epithelial cells. (**H**) ImageJ and GraphPad were used to compute the result G ($n = 3$ samples). Data were expressed as mean ± standard error of the mean. *$P < 0.05$, **$P < 0.01$, ***$P < 0.001$. Two-way ANOVA. Scale bars: (**A**) 100 μm, (**C**, **E**) 400 μm.

Investigative Ophthalmology & Visual Science

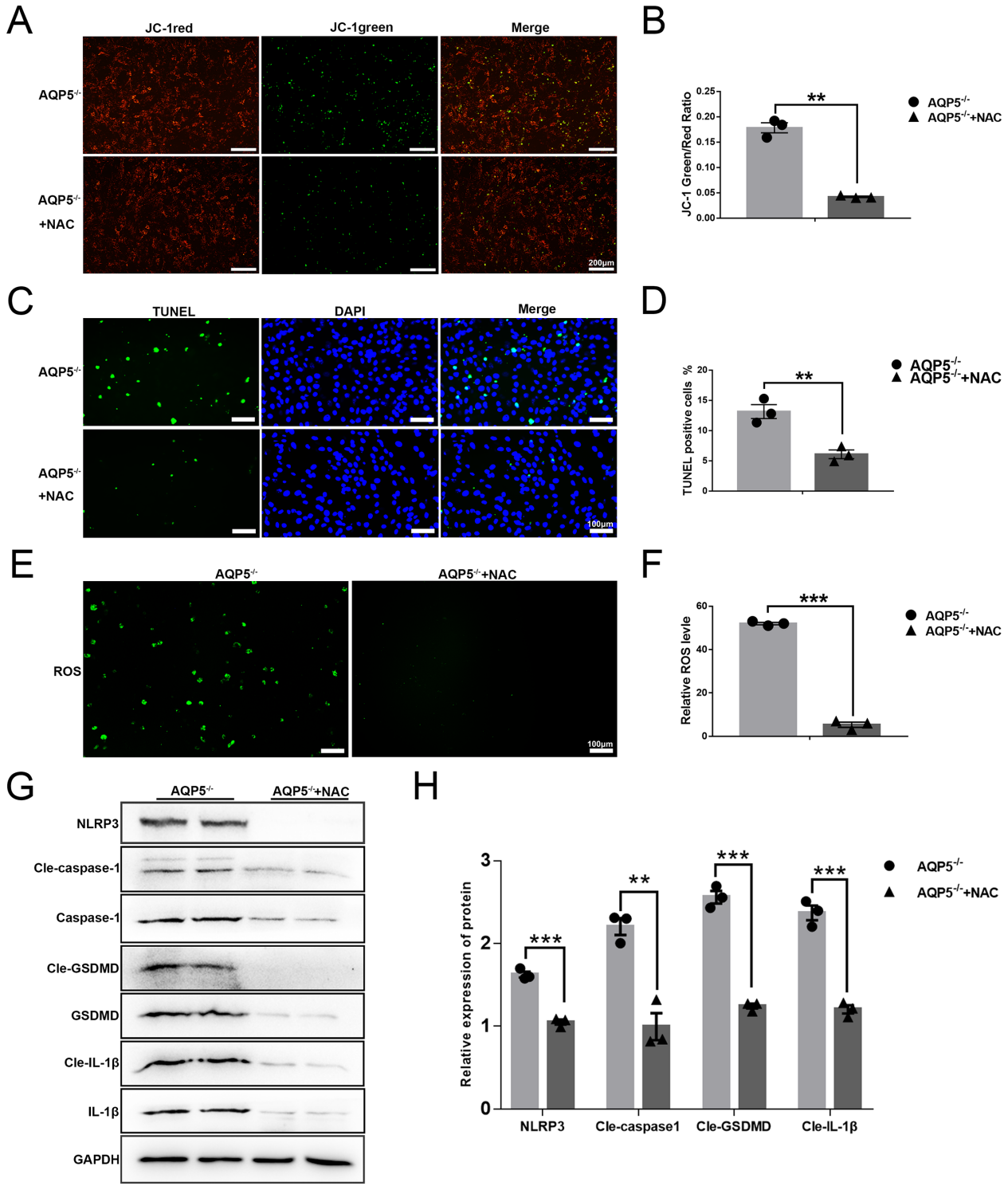


**Figure 7.** ROS removal decreased LG pyroptosis by inhibiting NLRP3 inflammasome activation. (**A**) JC-1 green/red ratio fluorescence staining of primary LG epithelial cells. (**B**) ImageJ immunofluorescence spectrum analysis showed the average fluorescence intensity of JC-1 green/red ratio ($n$ = 3 samples). Representative complete pictures of each sample were used for quantitative analysis. (**C**) TUNEL staining of primary LG epithelial cells (*green*, TUNEL; *blue*, DAPI). (**D**) ImageJ and GraphPad were used to calculate the result of **C** ($n$ = 3 samples). Representative complete pictures of each sample were used for quantitative analysis. (**E**) ROS immunofluorescence staining of primary LG epithelial cells (*green*). (**F**) ImageJ immunofluorescence spectrum analysis showed the average ROS fluorescence intensity ($n$ = 3 samples). Representative complete pictures of each sample were used for quantitative analysis. The number of ROS-positive cells in the AQP5$^{-/-}$ mice 52 ± 0.577 in the NAC-treated AQP5$^{-/-}$ mice 5.333 ± 1.202. (**G**) Western blotting showed the expression level of NLRP3, Cle-caspase-1, caspase-1, Cle-GSDMD, GSDMD, IL-1$\beta$, Cle-IL-1$\beta$, and GAPDH in primary LG epithelial cells. (**H**) ImageJ and GraphPad were used to compute the result of **G** ($n$ = 3 samples). Data were expressed as mean ± standard error of the mean. *$P$ < 0.05, **$P$ < 0.01, ***$P$ < 0.001. Two-way ANOVA. Scale bars: (**A**) 200 μm, (**C**, **E**) 100 μm.

Investigative Ophthalmology & Visual Science

in the MCC950-treated AQP5$^{-/-}$ mice. The MCC950-treated AQP5$^{-/-}$ mice had a lower green/red JC-1 ratio (3.367% ± 0.186%) than the AQP5$^{-/-}$ mice (13.400% ± 0.033%) ($P < 0.001$; $n = 3$ per group). Additionally, the MCC950-treated AQP5$^{+/+}$ mice had a lower green/red JC-1 ratio (1.233% ± 0.088%) than the AQP5$^{+/+}$ mice (1.900% ± 0.116%) ($P < 0.05$; $n = 3$ per group) (Fig. 6D). TUNEL staining revealed that the primary LG epithelial cells of the MCC950-treated AQP5$^{-/-}$ mice had a significantly lower number of TUNEL-positive stained cells than the AQP5$^{-/-}$ mice (Fig. 6E). The MCC950-treated AQP5$^{-/-}$ mice had a lower number of TUNEL-positive cells (4.3200% ± 0.1305%) than the AQP5$^{-/-}$ mice (15.460% ± 1.254%) ($P < 0.01$; $n = 3$ per group). Furthermore, the MCC950-treated AQP5$^{+/+}$ mice had a lower number of TUNEL-positive cells (1.83300% ± 0.08413%) than the AQP5$^{+/+}$ mice (2.5070% ± 0.1594%) ($P < 0.05$; $n = 3$ per group) (Fig. 6F). A Western blot analysis revealed that MCC950 reduced NLRP3 inflammasome activation, and show a notable decrease in Cle-caspase-1, Cle-GSDMD, and Cle-IL-1$\beta$ (Figs. 6G and 6H). These results were similar to those observed in the mouse LGs.

### ROS Removal Decreased LG Pyroptosis by Inhibiting the NLRP3 Inflammasome Activation

The NAC antioxidant was applied to assess the impact of ROS on the NLRP3 inflammasome and pyroptosis and to determine the association between oxidative stress and the NLRP3 inflammasome.[30] The primary LG epithelial cells were treated with 1 mM NAC for 24 hours. NAC alleviated the reversal of the MMP of the primary LG epithelial cells (Fig. 7A). The NAC-treated primary LG epithelial cells of AQP5$^{-/-}$ mice had a lower green/red JC-1 ratio (5.131% ± 0.100%) than the AQP5$^{-/-}$ mice (15.170% ± 4.446%) ($P < 0.01$; $n = 3$ per group) (Fig. 7B). TUNEL staining revealed that the NAC-treated primary LG epithelial cells of AQP5$^{-/-}$ mice had a significantly lower number of TUNEL-positive stained cells than the AQP5$^{-/-}$ mice (Fig. 7C). The number of TUNEL-positive cells decreased from 13.140% ± 1.149% in the primary LG epithelial cells of AQP5$^{-/-}$ mice to 6.0700% ± 0.7181% in the NAC-treated AQP5$^{-/-}$ mice ($P < 0.01$; $n = 3$ per group) (Fig. 7D). The ROS-positive cells were significantly decreased in the primary LG epithelial cells of NAC-treated AQP5$^{-/-}$ mice (Fig. 7E). The number of ROS-positive cells decreased from 52.000 ± 0.577 in the primary LG epithelial cells of AQP5$^{-/-}$ mice to 5.333 ± 1.202 in the NAC-treated AQP5$^{-/-}$ mice ($P < 0.001$; $n = 3$ per group) (Fig. 7F). A Western blot analysis revealed that the NAC-treated primary LG epithelial cells of AQP5$^{-/-}$ mice exhibited lower NLRP3 inflammasome activation and lower Cle-caspase-1, Cle-GSDMD, and Cle-IL-1$\beta$ expression levels than did the AQP5$^{-/-}$ mice (Figs. 7G and 7H).

## Discussion

The main feature of DED is the instability of the tear film's homeostasis, which can irritate the eye and ultimately impair vision.[31] The LGs generate an ocular-lubricating secretion that maximizes vision and supports ocular homeostasis. LG dysfunction can often be induced by Sjögren syndrome and trauma, which can result in LG pathologies such as DED.[32] More recently, the transplantation of ex vivo epithelial secretory cells or micro-organs/tissues into the damaged glands has been the main focus of prospective therapeutic techniques for restoring LG secretion.[33–37] Nevertheless, the pathogenic mechanisms of LG-associated DED are remain relatively unknown. The main finding of this work was that pyroptosis in LG epithelial cells resulted from NLRP3 inflammatory activation in AQP5$^{-/-}$ mice.

AQP5 is crucial in saliva secretion and is expressed in both the salivary glands and LGs. Sjögren syndrome destroys the salivary glands and LGs and it is associated with AQP5 deficiency.[38] In recent years, several AQPs have been discovered to transport $H_2O_2$.[12–14] Moreover, it has been confirmed that ROS, particularly $H_2O_2$, participate in cellular signaling pathways that affect cell growth and proliferation mechanisms and contribute to the development of diseases.[39,40] Numerous studies have revealed that ROS generation is an important factor in NLRP3 inflammasome activation.[22] Furthermore, DED is caused by ROS generation and NLRP3 inflammasome activation.[20] However, the accurate mechanism of inflammasomes in DED remains unknown. In this work, we discovered that the LGs of AQP5$^{-/-}$ mice had more ROS-positive cells than the LGs of AQP5$^{+/+}$ mice, as well as increased NLRP3 inflammasome activation.

Pyroptosis plays an influential role in tissue damage caused by inflammation.[41–43] The typical pyroptosis pathway is mainly triggered by caspase-1.[25] Studies have illustrated that GSDMD is downstream of NLRP3, and that GSDMD proteins undergo cleavage and pyroptosis after caspase-1 activation by inflammatory NLRP3. GSDMD is the enforcer of pyroptosis downstream of typical inflammasome pathways and is a substrate for inflammatory caspase-1.[27–29] The NLRP3 inflammasome and GSDMD play key roles in pyroptosis.[44] In this study, we discovered that the AQP5$^{-/-}$ mouse LGs had significantly higher GSDMD production than the AQP5$^{+/+}$ mouse LGs. The MCC950-treated AQP5$^{-/-}$ mice presented lower Cle-caspase-1, Cle-IL-1$\beta$, Cle-GSDMD, and NLRP3 inflammasome activities than the AQP5$^{-/-}$ mice. Moreover, the MCC950-treated LG epithelial cells exhibited relatively low Cle-caspase-1, Cle-IL-1$\beta$, Cle-GSDMD, and NLRP3 inflammasome activity. Our study results indicated that the LG epithelial cells in AQP5$^{-/-}$ mice undergo increased GSDMD-executed pyroptosis. Nevertheless, the contribution of pyroptosis to the etiopathogenesis of DED requires further investigation.

Cell culture is now widely used in various fields and dominates current experimental research.[45] Many of the behaviors of biological activities in the body, such as cell differentiation, migration, growth, and mechanisms, can be summarized in this way, which advances our understanding of cell behavior.[46] However, ROS production is difficult to detect in cryosections of the glands. According to the green fluorescence production in living cells, the contents and changes in ROS can be determined. Fluorescence microscopy can be observed directly and is considered the standard method for detecting ROS in living cells. We treated the primary LG epithelial cells of AQP5$^{-/-}$ mice with NAC to clarify whether the aggregation of ROS induced by AQP5 deficiency caused the elevation of NLRP3 and pyroptosis. NAC treatment significantly decreased the stress status of the primary LG epithelial cells of AQP5$^{-/-}$ mice, and it also decreased the activity of the NLRP3 inflammasome. These results hint that the pyroptosis of the primary LG epithelial cells of AQP5$^{-/-}$ mice was caused by an increase in ROS caused by AQP5 deficiency. The increase in ROS promoted NLRP3 inflammasome activation and inflammatory responses.

Investigative Ophthalmology & Visual Science

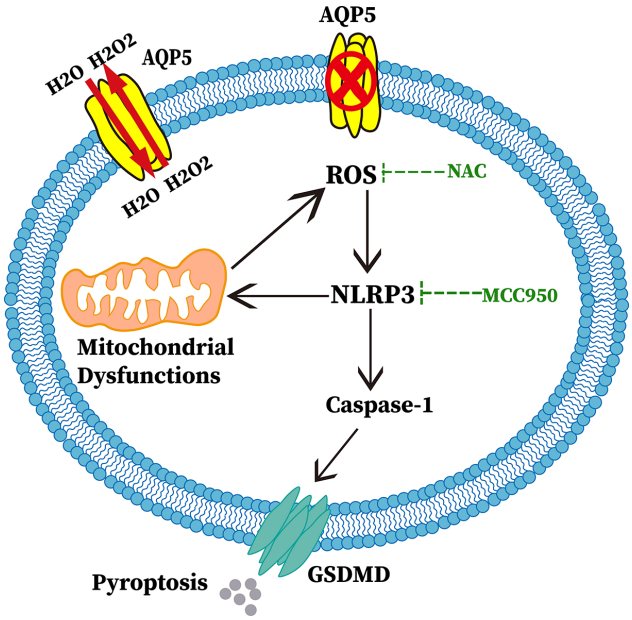


**Figure 8.** Modes of the AQP5/ROS/NLRP3 inflammasome axis leading to LGs pyroptosis.

Taken together, this study demonstrated the effect of NLRP3 inflammasome-mediated cell pyroptosis in AQP5$^{-/-}$ mouse LGs. We propose that the mass production of ROS in AQP5$^{-/-}$ mouse LGs results in cell oxidative stress, activates the NLRP3 inflammasome, induces mitochondrial dysfunction, and ultimately induces pyroptosis in LG acinar cells (Fig. 8). Pyroptosis in LGs could be reduced by pharmacologically blocking the NLRP3 inflammasome and removing ROS. Our findings emphasize the disease-producing effects of the AQP5/ROS/NLRP3 inflammasome axis in DED and provide a new therapeutic direction for DED research.

## *Acknowledgments*

The authors thank Editage for linguistic assistance during the preparation of this article.

Supported by the National Natural Science Foundation of China (No. 81970782), Shandong Provincial Natural Science Foundation grant (ZR2022MH183).

Disclosure: **X. Cao**, None; **G. Di**, None; **Y. Bai**, None; **K. Zhang**, None; **Y. Wang**, None; **H. Zhao**, None; **D. Wang**, None; **P. Chen**, None

## *References*

1. Shimazaki J. Definition and diagnostic criteria of dry eye disease: historical overview and future directions. *Invest Ophthalmol Vis Sci*. 2018;59:DES7–DES12.
2. Stapleton F, Alves M, Bunya VY, et al. TFOS DEWS II Epidemiology Report. *Ocular Surf*. 2017;15:334–365.
3. Huerva V, Ascaso FJ, Grzybowski A. Ocular inflammation. *Mediators Inflamm*. 2015;2015:398076.
4. Giasson BI, Duda JE, Murray IV, et al. Oxidative damage linked to neurodegeneration by selective alpha-synuclein nitration in synucleinopathy lesions. *Science (New York, NY)*. 2000;290:985–989.
5. Wakamatsu TH, Dogru M, Ayako I, et al. Evaluation of lipid oxidative stress status and inflammation in atopic ocular surface disease. *Mol Vis*. 2010;16:2465–2475.
6. Craig JP, Nelson JD, Azar DT, et al. TFOS DEWS II report executive summary. *Ocular Surf*. 2017;15:802–812.
7. Nakamura S, Shibuya M, Nakashima H, et al. Involvement of oxidative stress on corneal epithelial alterations in a blink-suppressed dry eye. *Invest Ophthalmol Vis Sci*. 2007;48:1552–1558.
8. Alishahi M, Kamali R. A novel molecular dynamics study of CO2 permeation through aquaporin-5. *Eur Phys J E*. 2019;42:151.
9. Kourghi M, Pei JV, De Ieso ML, Nourmohammadi S, Chow PH, Yool AJ. Fundamental structural and functional properties of Aquaporin ion channels found across the kingdoms of life. *Clin Exp Pharmacol Physiol*. 2018;45:401–409.
10. Verkman AS. Aquaporins: translating bench research to human disease. *J Exp Biol*. 2009;212:1707–1715.
11. Ishibashi K, Tanaka Y, Morishita Y. The role of mammalian superaquaporins inside the cell. *Biochim Biophys Acta Gen Subjects*. 2014;1840:1507–1512.
12. Bienert GP, Møller ALB, Kristiansen KA, et al. Specific aquaporins facilitate the diffusion of hydrogen peroxide across membranes*. *J Biol Chem*. 2007;282:1183–1192.
13. Rodrigues C, Mósca AF, Martins AP, et al. Rat aquaporin-5 Is pH-gated induced by phosphorylation and is implicated in oxidative stress. *Int J Mol Sci*. 2016;17:2090.
14. Rodrigues C, Pimpão C, Mósca AF, et al. Human Aquaporin-5 facilitates hydrogen peroxide permeation affecting adaption to oxidative stress and cancer cell migration. *Cancers (Basel)*. 2019;11:932.
15. Raina S, Preston GM, Guggino WB, Agre P. Molecular cloning and characterization of an aquaporin cDNA from salivary, lacrimal, and respiratory tissues (∗). *J Biol Chem*. 1995;270:1908–1912.
16. Moore M, Ma T, Yang B, Verkman AS. Tear secretion by lacrimal glands in transgenic mice lacking water channels AQP1, AQP3, AQP4 and AQP5. *Exp Eye Res*. 2000;70:557–562.
17. Tsubota K, Hirai S, King LS, Agre P, Ishida N. Defective cellular trafficking of lacrimal gland aquaporin-5 in Sjögren's syndrome. *Lancet*. 2001;357:688–689.
18. Kumari SS, Varadaraj M, Menon AG, Varadaraj K. Aquaporin 5 promotes corneal wound healing. *Exp Eye Res*. 2018;172:152–158.
19. Lamkanfi M, Dixit VM. Inflammasomes: guardians of cytosolic sanctity. *Immunol Rev*. 2009;227:95–105.
20. Zheng Q, Ren Y, Reinach PS, et al. Reactive oxygen species activated NLRP3 inflammasomes prime environment-induced murine dry eye. *Exp Eye Res*. 2014;125:1–8.
21. Niu L, Zhang S, Wu J, Chen L, Wang Y. Upregulation of NLRP3 inflammasome in the tears and ocular surface of dry eye patients. *PLoS One*. 2015;10:e0126277.
22. Bauernfeind F, Bartok E, Rieger A, Franchi L, Núñez G, Hornung V. Cutting edge: reactive oxygen species inhibitors block priming, but not activation, of the NLRP3 inflammasome. *J Immunol*. 2011;187:613–617.
23. Zheng Q, Tan Q, Ren Y, et al. Hyperosmotic stress–induced TRPM2 channel activation stimulates NLRP3 inflammasome activity in primary human corneal epithelial cells. *Invest Ophthalmol Vis Sci*. 2018;59:3259–3268.
24. Uchino Y, Kawakita T, Miyazawa M, et al. Oxidative stress induced inflammation initiates functional decline of tear production. *PLoS One*. 2012;7:e45805.
25. Vande Walle L, Lamkanfi M. Pyroptosis. *Curr Biol*. 2016;26:R568–R572.
26. Xue Y, Enosi Tuipulotu D, Tan WH, Kay C, Man SM. Emerging activators and regulators of inflammasomes and pyroptosis. *Trends Immunol*. 2019;40:1035–1052.

27. He WT, Wan H, Hu L, et al. Gasdermin D is an executor of pyroptosis and required for interleukin-1$\beta$ secretion. *Cell Res*. 2015;25:1285–1298.
28. Shi J, Zhao Y, Wang K, et al. Cleavage of GSDMD by inflammatory caspases determines pyroptotic cell death. *Nature*. 2015;526:660–665.
29. Kayagaki N, Stowe IB, Lee BL, et al. Caspase-11 cleaves gasdermin D for non-canonical inflammasome signalling. *Nature*. 2015;526:666–671.
30. Wan L, Bai X, Zhou Q, et al. The advanced glycation end-products (AGEs)/ROS/NLRP3 inflammasome axis contributes to delayed diabetic corneal wound healing and nerve regeneration. *Int J Biol Sci*. 2022;18:809–825.
31. Craig JP, Nichols KK, Akpek EK, et al. TFOS DEWS II definition and classification report. *Ocular Surf*. 2017;15:276–283.
32. Bron AJ, de Paiva CS, Chauhan SK, et al. TFOS DEWS II pathophysiology report. *Ocular Surf*. 2017;15:438–510.
33. Tiwari S, Nair RM, Vamadevan P, et al. Establishing and characterizing lacrispheres from human lacrimal gland for potential clinical application. *Graefe's Arch Clin Exp Ophthalmol*. 2018;256:717–727.
34. Hirayama M, Tsubota K, Tsuji T. Generation of a bioengineered lacrimal gland by using the organ germ method. In: Tsuji T (ed), *Organ Regeneration: 3D Stem Cell Culture & Manipulation*. New York: Springer; 2017:153–165.
35. Hirayama M, Ogawa M, Oshima M, et al. Functional lacrimal gland regeneration by transplantation of a bioengineered organ germ. *Nat Commun*. 2013;4:2497.
36. Gromova A, Voronov DA, Yoshida M, et al. Lacrimal gland repair using progenitor cells. *Stem Cells Transl Med*. 2017;6:88–98.
37. Brockes JP, Kumar A. Appendage regeneration in adult vertebrates and implications for regenerative medicine. *Science*. 2005;310:1919–1923.
38. Delporte C, Bryla A, Perret J. Aquaporins in salivary glands: from basic research to clinical applications. *Int J Mol Sci*. 2016;17:166.
39. Rhee SG. Cell signaling. H2O2, a necessary evil for cell signaling. *Science*. 2006;312:1882–1883.
40. Dickinson BC, Chang CJ. Chemistry and biology of reactive oxygen species in signaling or stress responses. *Nat Chem Biol*. 2011;7:504–511.
41. Miao EA, Leaf IA, Treuting PM, et al. Caspase-1-induced pyroptosis is an innate immune effector mechanism against intracellular bacteria. *Nat Immunol*. 2010;11:1136–1142.
42. Hett EC, Slater LH, Mark KG, et al. Chemical genetics reveals a kinase-independent role for protein kinase R in pyroptosis. *Nat Chem Biol*. 2013;9:398–405.
43. Cookson BT, Brennan MA. Pro-inflammatory programmed cell death. *Trends Microbiol*. 2001;9:113–114.
44. Xia X, Wang X, Cheng Z, et al. The role of pyroptosis in cancer: pro-cancer or pro-"host"? *Cell Death Dis*. 2019;10:650.
45. Duval K, Grover H, Han LH, et al. Modeling physiological events in 2D vs. 3D cell culture. *Physiology (Bethesda, Md)*. 2017;32:266–277.
46. Huh D, Hamilton GA, Ingber DE. From 3D cell culture to organs-on-chips. *Trends Cell Biol*. 2011;21:745–754.